Thermally Stratified Liquid Turbulence with a Chemical Reaction

Ryo Onishi and Satoru Komori
Dept. of Mechanical Engineering and Science, Kyoto University, Kyoto 606-8501, Japan

DOI 10.1002/aic.10675
Published online September 21, 2005 in Wiley InterScience (www.interscience.wiley.com).

Effects of stable and unstable thermal stratifications on turbulent mixing and chemical reaction in liquid turbulence were investigated by both laboratory experiments and numerical simulations. Instantaneous velocity and concentration were simultaneously measured using a combined technique with a two-component laser-Doppler velocimeter (LDV) and a laser-induced fluorescence (LIF) method in two kinds of thermally stratified turbulent reacting flows: grid-generated turbulence and a mixing layer. The results show that turbulent mixing in the fully developed liquid turbulence is affected mainly at large scales by buoyancy. However, the maximum value of the mean concentration of chemical product is independent of thermal stratification. In addition, a large-eddy simulation (LES) based on a β-pdf model was applied to the same thermally stratified reacting liquid flows as used in the experiments. The numerical results show that the stratification effects on the turbulent mixing and chemical reaction can be well predicted by the LES and the buoyancy effects are not significant in the subgrid-scale models for the LES. © 2005 American Institute of Chemical Engineers *AIChE J,* 52: 456–468, 2006
Keywords: laser-Doppler velocimetry, laser-induced fluorescence, large-eddy simulation, subgrid-scale model, thermal stratification, turbulent mixing

Introduction

Turbulent reacting flows can be seen not only in industrial plants such as combustors or reactors but also in environmental flows. When flows are density stratified, turbulent reactive–diffusive mechanism will be influenced by buoyancy. It is thus of great importance to clarify the buoyancy effects for both designing high-performance industrial reactors and predicting the turbulent diffusion of reactive contaminants in environmental flows.

To clarify the turbulent mixing and chemical reaction processes experimentally, we need sophisticated techniques for measuring instantaneous velocity and concentration with good spatial and temporal resolutions comparable to the Kolmogorov scale and the Batchelor scale, respectively. However, the Batchelor scale is defined by dividing the Kolmogorov scale by the square root of the Schmidt number and so the Batchelor scale is one order smaller in liquid turbulence than that in gas turbulence, given that the Schmidt number is two orders higher in liquid flow than that in gas flow. The extremely small Batchelor scale in liquid turbulence makes it hard to measure instantaneous concentration with good accuracy, and thus the number of published experimental studies on the turbulent mixing and chemical reaction in liquid flows is limited. Nagata and Komori[1] investigated the reactive–diffusive mechanism in liquid grid-generated turbulence and further investigated the unstable stratification effect on the chemical reaction. However, there has been no study on the buoyancy effect in stably stratified reacting grid-generated turbulence. As for the liquid shear turbulence, Koochesfahari and Dimotakis,[2] Broadwell and Mungal,[3] and others investigated the reactive–diffusive mechanism in the neutral liquid mixing layer, but no one has investigated the buoyancy effects on the reactive–diffusive mechanism in the stratified liquid mixing layer. Thus, experimental investigations on the buoyancy effects in stratified reacting liquid turbulence remain to be carried out.

Correspondence concerning this article should be addressed to S. Komori at komori@mech.kyoto-u.ac.jp.

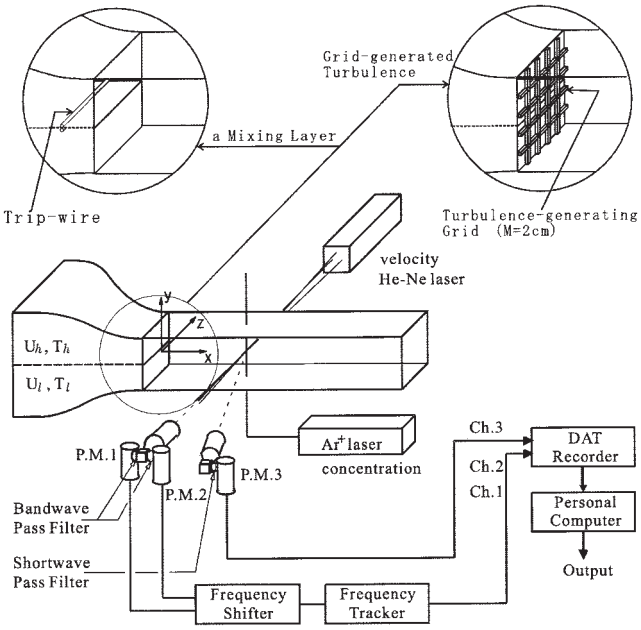

Figure 1. Experimental apparatus and measuring system.

On the other hand, numerical simulation can also play an important role in investigating the reacting turbulence because it enables us to predict various turbulence quantities that we can hardly measure. Therefore, it is of great importance to develop a reliable numerical simulation technique that can well predict buoyancy effects on turbulent diffusive–reactive mechanism. Recently, direct numerical simulation (DNS) has often been applied to reacting turbulence. However, the DNS is applicable only to low Reynolds number (Re) or low Schmidt number (Sc) flows because it requires high spatial and temporal resolutions corresponding to the Batchelor scale and therefore it is impossible to apply the DNS to reacting liquid turbulence with high Reynolds numbers. With respect to this point, large-eddy simulation (LES) seems to be a more practical simulation method than the DNS. In the LES, the grid scale (GS) values that can be resolved by the numerical grids are directly computed and the subgrid scale (SGS) values that cannot be resolved are estimated with SGS models. Because we can set the numerical grid width much larger than the Kolmogorov and Batchelor scales, we can apply the LES to high Reynolds number and high Schmidt number flows. To exploit this advantage of the LES, we have to develop appropriate SGS models. However, the SGS model for the reaction source term in liquid turbulence is still in a developmental stage. Recently Michioka and Komori[4] proposed a simple SGS model for the reaction source term in liquid turbulence, based on the β-pdf model developed by Cook and Riley,[5] and they have shown its good applicability by comparisons with the experimental data. However, they have verified the applicability only in the neutrally stratified case and have not applied their LES to stratified reacting liquid turbulence.

The purpose of this study is, therefore, to experimentally clarify the buoyancy effects on the reactive–diffusive mechanism in thermally stratified reacting liquid turbulence and to develop the LES that is applicable to thermally stratified reacting liquid flows.

Table 1. Experimental Conditions for Grid-Generated Liquid Turbulence

Case	U_0 (m/s)	ΔT (K) ($T_h - T_l$)
Neutrally stratified	0.180	0
Unstably stratified	0.180	−10
Stably stratified	0.180	10

Experimental

In this study, two types of reacting liquid turbulence were investigated: (1) grid-generated turbulence and (2) the turbulent mixing layer. Figure 1 shows a schematic of the experimental apparatus and measuring system. The test apparatus used was a rectangular water tunnel made of polymethylmethacrylate (PMMA), 1.0 m in length and 0.1 × 0.1 m in cross section. The upper and lower fluid streams are separated by a splitter plate before entering into the test section. The coordinate system used was as follows: x is the streamwise distance from the entrance of the test section; y and z are the vertical and spanwise distances from the center of the cross section of the channel, respectively.

To form reacting grid-generated liquid turbulence, a turbulence-generating grid of square-rod, square-mesh, and single-monoplane construction was installed at the entrance to the test section. The mesh size M and length of a side of the rod d were 2.0×10^{-2} and 2.0×10^{-3} m, respectively. For reacting liquid mixing layer, a couple of trip wires were mounted on both sides of the splitter plate at 0.06 m upstream from the tail end. The trip wires were 1.2 mm in diameter and were used to obtain the fully developed mixing layer.[6,7]

To produce thermally stratified flows, water in either the upper or the lower stream was heated by a boiler and the temperature was regulated to a constant value in the storage tank within ±0.1 K by using an electric heater connected to a temperature-control unit (Technos BC-130-S, Sinko Co. Ltd., Guangdong, China).

The experimental conditions for the grid-generated turbulence and mixing layer are listed in Tables 1 and 2, respectively. The temperature difference between upper and lower streams in thermally stratified cases was set to 10 K. The greater temperature difference is more suitable for observing stratification effects. However, the greater temperature difference leads to stronger variations of laser beam arising from the fluctuating refractive index, thus leading to substantial errors in concentration measurements by the laser-induced fluorescence (LIF) method. The value of 10 K was the limit of temperature difference that not only allows strong thermal stratifications but also ensures the accuracy of concentration measurements. The standard deviations of the measurements of mean concentra-

Table 2. Experimental Conditions for a Liquid Mixing Layer

Case	U_{ave} (m/s)	ΔU (m/s) ($U_h - U_l$)	ΔT (K) ($T_h - T_l$)
Neutrally stratified	0.125	0.080	0
Unstably stratified	0.125	0.080	−10
Stably stratified	0.125	0.080	10

Table 3. Combinations of Species A and B

Flow Type	Species A (Lower Stream)	Species B (Upper Stream)
Nonreacting flow	H_2O	H_2O + uranine
Reacting flow	CH_3COOH + uranine	NH_4OH + uranine

tions in the central region were within 4% in the stably and unstably stratified cases and within 2% in the neutral case. In the grid-generated turbulence case, the Reynolds number based on the mesh size (Re_M) was 3.6×10^{-3}. The bulk Richardson numbers, $Ri_b(=]-\beta g \Delta TM/U_0^2)$, were 1.4×10^{-2} and -1.4×10^{-2} in the stable and unstable cases, respectively.

The combinations of species A in the lower stream and species B in the upper stream before mixing are listed in Table 3. For a nonreacting flow, fresh water without any chemical species was used as species A and fresh water with sodium fluorescein dye, uranine ($C_{20}H_{10}Na_2O_5$), was used as species B. For a reacting flow, acetic acid (CH_3COOH) and ammonium hydroxide (NH_4OH) were used as species A and B, respectively. The neutralization reaction between the weak acid and base is expressed as an irreversible second-order rapid reaction:

$$CH_3COOH + NH_4OH \rightarrow CH_3COONH_4 + H_2O \quad (1)$$

The reaction rate constant k_r was of the order 10^8 m^3 mol^{-1} s^{-1}. The initial concentrations of the two reacting species, C_{A0} and C_{B0}, were determined to be the same values of 0.01 mol m^{-3} to measure the concentration by means of a LIF method based on the dependency of fluorescence intensity on the pH of the solution. The change of temperature arising from the reaction was negligibly small because the concentrations of reacting species used here were extremely low.

Instantaneous velocities in the streamwise and vertical directions were measured using a two-component laser-Doppler velocimeter (LDV). The LDV used was a Dantec 55X modular system (Dantec Dynamics A/S, Skovlunde, Denmark) with a polarization beam splitter (55X24), a 40-MHz Bragg cell, and the laser was a 5-mW He–Ne laser (wave length: $\lambda = 632.8$ nm; model 106-1, Spectra Physics, Inc., Mountain View, CA). The He–Ne laser beams were introduced from the sidewall of the test section. The spatial resolution of the LDV was approximately 500 microns, which was sufficiently fine to resolve fluid motions at the dissipation scale.

Instantaneous concentrations of reacting and nonreacting species were measured using a LIF method and the concentration and velocity measurements by the LIF and LDV were simultaneously carried out at the same measuring point. For the concentration measurement by the LIF method, the uranine diffusing in the flow was illuminated by a high-power single-line mode argon-ion (Ar^+) laser ($\lambda = 488.0$ nm; model 95-4, Lexel Lasers, Fremont, CA) with 0.8 W power. The Ar^+ laser beam was introduced through the bottom wall of the test section and it was focused on the measuring point. The fluorescence from the measuring point was collected using the same optical system as that used in Komori et al.[8] and was detected by a photomultiplier. For a nonreacting flow, instantaneous concentration of the uranine, which was initially premixed in the upper stream, was measured as the instantaneous concentration of a nonreacting species B, C_B^*, using a proportional calibration curve between the LIF intensity and the concentration of the uranine. Hereafter, the asterisk denotes the concentration in the nonreacting case.

The reason that the uranine was initially premixed in the upper stream was to reduce the attenuation along the path of the laser beam introduced from the bottom wall. From the concentration of nonreacting species B, instantaneous concentration of nonreacting species A, C_A^*, was determined by $C_A^*/C_{A0} = 1 - C_B^*/C_{A0}$. For a reacting flow, the uranine was initially premixed in both upper and lower streams at a constant concentration and the dependency of the LIF intensity on the pH of the solution was used to measure C_A. The LIF intensity from the uranine premixed at a constant concentration does not change in neutral or basic solution (pH $\geq$ 7), but it decays depending on the concentration of the weak acid in the side of pH $<$ 7. Therefore, a nonlinear calibration curve between the LIF intensity and the concentration of the acetic acid was obtained in a well-mixed tank.[8] The instantaneous concentration of reacting species A, C_A, was directly measured from the LIF intensity with the calibration curve. The spatial resolution of the LIF method was approximately 80 microns and it enabled us to use the calibration curve. The accuracy of this concentration measurement method has been fully described in Komori et al.[9]

A cold-film I probe of 10 μm diameter (model 1260-10W, TSI Inc., Shoreview, MN) operated by a constant-current temperature bridge (Dantec 55M) was used to measure the instantaneous temperature in thermally stratified flows.

The sampling frequency and size for the concentration and velocity signals were 2.0 kHz and 80,000 points, respectively. The digitized data were recorded by a data recorder (model PC208AX, Sony Corp., Tokyo, Japan), and statistical processing of the data was performed by a personal computer.

Large-Eddy Simulation

LES of thermally stratified liquid turbulence with a chemical reaction

The governing equations are the continuity equation, the Navier–Stokes equation, and the transport equations for heat and mass. Filtered governing equations can be written as

$$\frac{\partial \bar{U}_i}{\partial x_i} = 0 \quad (2)$$

$$\frac{\partial \bar{U}_i}{\partial t} + \bar{U}_j \frac{\partial \bar{U}_i}{\partial x_j} = -\frac{1}{\rho}\frac{\partial \bar{P}}{\partial x_i} + \nu \frac{\partial^2 \bar{U}_i}{\partial x_j \partial x_j} - \frac{\partial \tau_{ij}}{\partial x_j} - \beta g_i(\bar{T} - T_s) \quad (3)$$

$$\frac{\partial \bar{T}}{\partial t} + \bar{U}_j \frac{\partial \bar{T}}{\partial x_j} = \frac{\nu}{\mathrm{Pr}} \frac{\partial^2 \bar{T}}{\partial x_j \partial x_j} - \frac{\partial h_j}{\partial x_j} \quad (4)$$

$$\frac{\partial \bar{C}_i}{\partial t} + \bar{U}_j \frac{\partial \bar{C}_i}{\partial x_j} = \frac{\nu}{\mathrm{Sc}} \frac{\partial^2 \bar{C}_i}{\partial x_j \partial x_j} - \frac{\partial q_{ij}}{\partial x_j} + \bar{\omega} \quad (5)$$

where an overbar denotes the filtered value. Here, a simple second-order Gaussian filter was used. The unresolved subgrid scale (SGS) effects appear in the SGS stress term τ_{ij}, the SGS

heat flux term h_j, the SGS mass flux term q_{ij}, and the filtered chemical reaction source term $\bar{\omega}$. In this study, dynamic SGS models were used for the SGS Reynolds stress and the SGS heat and mass fluxes.

Modeling of buoyancy effect on SGS flow field

A conventional dynamic Smagorinsky model[10] for the SGS Reynolds stress assumes that energy production by shear is equal to energy dissipation. From this assumption, we can derive

$$\tau_{ij} - \frac{1}{3}\,\delta_{ij}\tau_{kk} = -2C\bar{\Delta}^2|\bar{S}|\bar{S}_{ij} \tag{6}$$

where $\overline{S_{ij}} = [(\partial \bar{U}_i/\partial x_j) + (\partial \bar{U}_j/\partial x_i)]/2$ and C is a coefficient, which can be dynamically determined from grid-scale (GS) quantities.

In thermally stratified flows, buoyancy may directly influence the SGS flow field. Especially in liquid flows, the buoyancy effect may be significant because of its high Prandtl number. Wong and Lilly[11] assumed that energy productions by shear and buoyancy are balanced with energy dissipation, and then they could derive

$$\tau_{ij} - \frac{1}{3}\,\delta_{ij}\tau_{kk} = -2\nu_{SGS}\bar{S}_{ij} = -2C\bar{\Delta}^2\left(1 + \frac{g_i\beta}{\mathrm{Pr}_{SGS}|\bar{S}|^2}\frac{\partial \bar{T}}{\partial x_i}\right)^{1/2}|\bar{S}|\bar{S}_{ij} \tag{7}$$

We carried out the two large-eddy simulations based on the two SGS stress models of Eqs. 6 and 7, and discussed the buoyancy effect on the SGS flow field by comparing two LES predictions.

For the filtered reaction source term, we used the SGS model proposed by Michioka and Komori.[4] The details are described in the following subsection.

SGS model for a rapid reaction

A second-order rapid reaction (A + B $\rightarrow$ P) between acetic acid and ammonium hydroxide was used in the present experiments. In the rapid reaction, a timescale of chemical reaction is far smaller than that of turbulent diffusion. However, such a sufficiently fine time resolution for the reaction timescale is not feasible even with the most advanced supercomputer. Therefore, Cook and Riley[5] developed an SGS model for the rapid reaction by introducing a conserved scalar. The conserved scalar is defined by

$$Z = C_A - C_B = C_A^* - C_B^* \tag{8}$$

A normalized conserved scalar ζ is defined by

$$\zeta = \frac{Z - Z_{B0}}{Z_{A0} - Z_{B0}} \tag{9}$$

where Z_{A0} and Z_{B0} are the initial values given by $Z_{A0} = C_{A0}$ and $Z_{B0} = -C_{B0}$. The conservation equation of the filtered ζ is

$$\frac{\partial \bar{\zeta}}{\partial t} + \bar{U}_j\frac{\partial \bar{\zeta}}{\partial x_j} = \frac{\nu}{\mathrm{Sc}}\frac{\partial^2\bar{\zeta}}{\partial x_j\partial x_j} - \frac{\partial q_j}{\partial x_j} \tag{10}$$

Assuming equilibrium chemistry, the concentration of all species in a nonpremixed, single-step reaction can be directly related to ζ by

$$C_A(\zeta)/C_{A0} = \begin{cases} 0 & (\zeta \le \zeta_{st}) \\ \dfrac{\zeta - \zeta_{st}}{1 - \zeta_{st}} & (\zeta > \zeta_{st}) \end{cases} \tag{11}$$

$$C_B(\zeta)/C_{A0} = \begin{cases} \dfrac{\zeta - \zeta_{st}}{1 - \zeta_{st}} & (\zeta \le \zeta_{st}) \\ 0 & (\zeta > \zeta_{st}) \end{cases} \tag{12}$$

$$C_P(\zeta)/C_{A0} = \begin{cases} \dfrac{\zeta}{\zeta_{st}} & (\zeta \le \zeta_{st}) \\ \dfrac{1 - \zeta}{1 - \zeta_{st}} & (\zeta > \zeta_{st}) \end{cases} \tag{13}$$

where

$$\zeta_{st} = \frac{C_{B0}}{C_{A0} + C_{B0}} \tag{14}$$

The value of ζ_{st} in the preceding equations was 0.5 in our study because we used the same initial concentrations of species A and B, that is, $C_{A0} = C_{B0}$.

The substitution of $\bar{\zeta}$ into ζ in Eqs. 11–13 means the neglect of the mixing process of chemical species in SGS, that is, the introduction of the well-mixed condition in SGS. Taking into account the SGS mixing, the GS concentrations can be computed by using the probability density function (PDF) of ζ:

$$\bar{C}_i = \int_0^1 C_i(\zeta)\mathrm{P}(\zeta)d\zeta \tag{15}$$

The probability density function $\mathrm{P}(\zeta)$ was given by the PDF model proposed by Girimaji[12]:

$$\mathrm{P}(\zeta) = \frac{\zeta^{a-1}(1-\zeta)^{b-1}}{B(a,b)} \tag{16}$$

where

$$a = \bar{\zeta}\left(\frac{\bar{\zeta}(1-\bar{\zeta})}{\overline{\zeta'^2}} - 1\right) \qquad b = (a/\bar{\zeta}) - a$$

$$B(a,b) = \int_0^1 \zeta^{a-1}(1-\zeta)^{b-1}d\zeta$$

The SGS variance of ζ, $\overline{\zeta'^2}$, cannot be obtained directly from the filtered ζ conservation equation (Eq. 10) and it cannot be

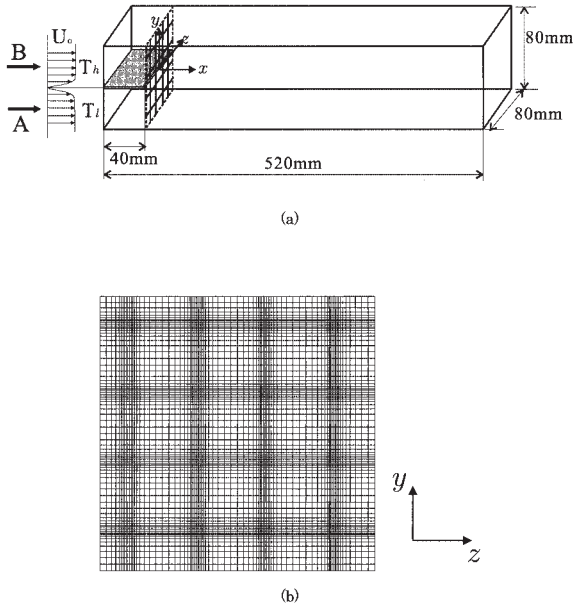

Figure 2. (a) The computational domain and (b) a profile of the numerical grid arrangement for the LES of the grid-generated turbulence.

assumed to be equal to the GS fluctuation, $\bar{\zeta}'^2$, especially in liquid turbulence because of its high Sc number. To consider the SGS effect, the SGS variance was assumed to be correlated with a test-scale variance as

$$\overline{\zeta^2} \approx c_f \widetilde{\zeta'^2} \tag{17}$$

where the tilde ($\tilde{}$) indicates the test-scale filtered value. The scale of the test-filter used was twofold larger than the scale of the normal SGS filter ($\tilde{\Delta} = 2\bar{\Delta}$). Cook and Riley[5] proposed an assumption of $c_f = 1.0$ in Eq. 17. On the other hand, Michioka and Komori[4] showed that the assumption of $c_f = 1.0$ is not valid in liquid turbulence. They investigated the value of c_f by carrying out the LES in various flows and found that the assumption of $c_f = 5.0$ is the best in liquid turbulence independently of flow types. However, this SGS model for SGS mixing has not been applied to density-stratified flows and its applicability has not been explicitly confirmed. Therefore, it is interesting and important to investigate whether the above SGS model is really applicable to stratified flows.

Computational method

The governing equations for the LES are given by Eqs. 2, 3, 4, and 10. Those equations were discretized on the staggered-mesh arrangement to construct a finite-difference formation. The HSMAC (highly simplified marker and cell) method[13] was used to solve the discretized equations. The reliability of the HSMAC method was confirmed by Nagata and Komori.[14] The second-order central difference method and the second-order Runge–Kutta method were used to calculate the spatial derivatives and the time integration, respectively. We used dynamic SGS models for the SGS Reynolds stress and the SGS turbulent mass and heat fluxes. The dynamic models often cause numerical instabilities because of negative values of turbulent diffusion coefficients. To stabilize the simulation, we used spanwise averaging on the turbulent diffusion coefficients.

The LES was carried out under the same conditions used in the experiments (see Tables 1 and 2). The kinematic viscosity ν and the thermal volumetric expansion coefficient β were given by the values at 298 K, corresponding to the cross-sectional mean water temperature used in the experiments. The Schmidt number (Sc) and the Prandtl number (Pr) were set at 600 and 5.0, respectively.

Figures 2a and 2b show the schematic diagram of the computational domain and a profile of the numerical grid arrangement for grid-generated turbulence. The computational domain was $520 \times 80 \times 80$ mm^3 and the number of grid points was $560 \times 80 \times 80$. The turbulence-generating grid with the same shape and dimension as those used in the experiments was installed in the computational domain. As shown in Figure 2b, the computational grids were irregularly and densely arranged near the turbulence-generating grid and splitter plate using a hyperbolic tangent function. The minimum and maximum grid widths were about 0.5 and 2.4 mm, respectively. The slip boundary conditions were imposed on the velocity components on the upper, lower, and side walls because the computational domain was smaller than the experimental one. A convective outlet boundary condition was used at the outlet boundary.

Figures 3a and 3b show the schematic diagram of the computational domain and a profile of the numerical grid arrangement for the mixing layer. In the neutrally and stably stratified cases, the computational domain was $480 \times 80 \times 80$ mm^3 in the streamwise, vertical, and spanwise directions and the number of grid points was $360 \times 60 \times 60$. In the unstably stratified case, the domain was set at $480 \times 106 \times 80$ mm^3 and the number of grid points was set at $360 \times 80 \times 60$ because the

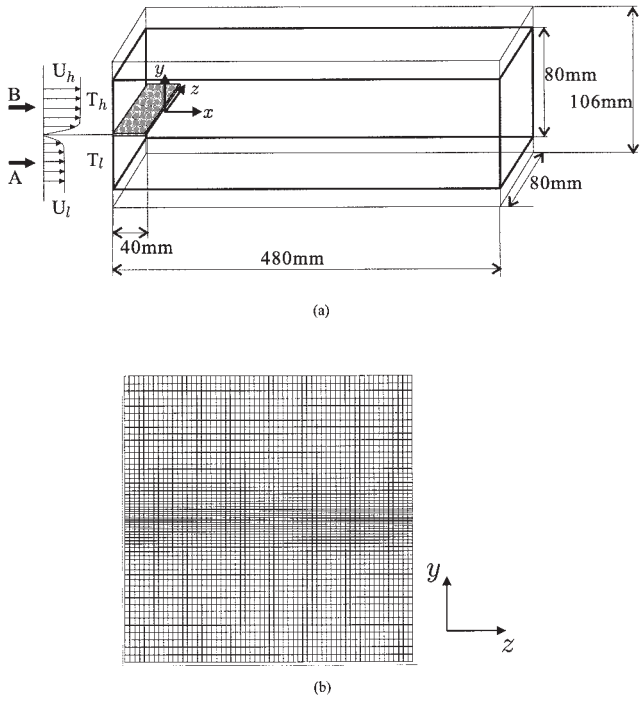

Figure 3. (a) The computational domain and (b) a profile of the numerical grid arrangement for the LES of the mixing layer.

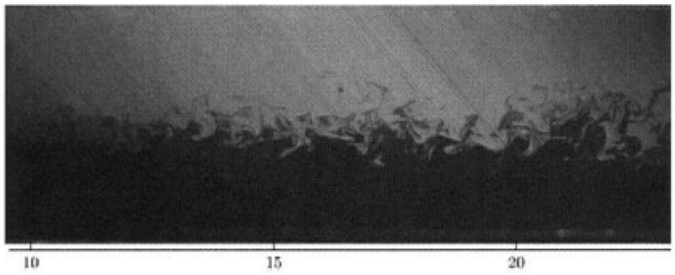

Figure 4. Instantaneous concentration field obtained (a) by the experiment with the LIF method and (b) by the LES, in the neutrally stratified grid-generated turbulence.

The upper stream is illuminated in both figures.

mixing region is enlarged vertically. To set the computational conditions equivalent to the experimental conditions, the splitter plate with 40 mm length was installed in the computational domain. The flow near the splitter plate was assumed to be a fully developed turbulent boundary layer because trip wires were mounted on the splitter plate in the experiments to quickly develop the turbulence. Therefore, the mean velocity distribution $\langle U_i(y)\rangle$ near the splitter plate was given by the same profile as that obtained by Spalart[15] in the fully developed turbulent boundary layer. Then, the random perturbation u_i was given in the sinusoidal form

$$u_i(y, z, t) = \sum_{n=1}^{20} u_{rms,i}(y)\sin[2\pi n f_0 t + \phi_i(y, z, nf_0)] \quad (18)$$

and the instantaneous velocity U_i was obtained by

$$U_i(x, y, z) = \langle U_i(y)\rangle + u_i(y, z, t) \quad (19)$$

Here, $u_{rms,i}$ is the root-mean-squared (rms) value of the turbulence intensity, f_0 is the basic frequency of 1 Hz, and ϕ_i is the uniformly distributed random number between 0 and 1. The maximum rms value of turbulence intensity was set at 10% of the mean velocity and its profile was given by Spalart.[15] The computational grids were arranged to be regular in the x- and z-directions and irregular in the y-direction. The grid width in the y-direction was set to smaller values near the splitter plate, as shown in Figure 3b. The grid width reached its minimum value of about 0.6 mm in the immediate vicinity of the plate. The same boundary conditions as those in the grid-generated turbulence case were imposed on the upper, lower, and side walls and at the outlet boundary.

Results and Discussion

Grid-generated turbulence

Figures 4a and 4b show the visualized concentration fields obtained by the experiment and by the LES in the neutrally stratified grid-generated turbulence. In the experiment, the upper fluid was illuminated by the LIF method with an Ar^+ laser sheet. The interface between the upper and lower streams is very clear in Figure 4a, which shows that the concentration gradient is sharp as a result of the small molecular diffusion in the liquid phase. In contrast to the clear interface by the experiment, the interface predicted by the LES is obscure because of the coarse grid resolution. However, we can see that the LES well predicts the large-scale mixing.

Figure 5 shows the streamwise distributions of the turbulence intensity of vertical velocity fluctuation on the center line ($y/M = z/M = 0$) in grid-generated turbulence, normalized by

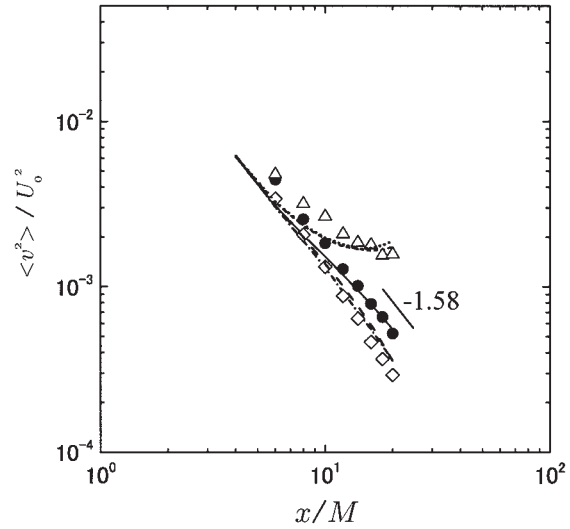

Figure 5. Streamwise distributions of the turbulence intensity of vertical velocity fluctuation in the grid-generated turbulence.

Symbols denote the measurements and lines denote the predictions by the two LES based on Eqs. 6 and 7: ●, —(Eq. 6), in the neutrally stratified case; △, - - - (Eq. 6), · · · (Eq. 7), in the unstably stratified case; ◇, – – –(Eq. 6), – – – (Eq. 7), in the stably stratified case.

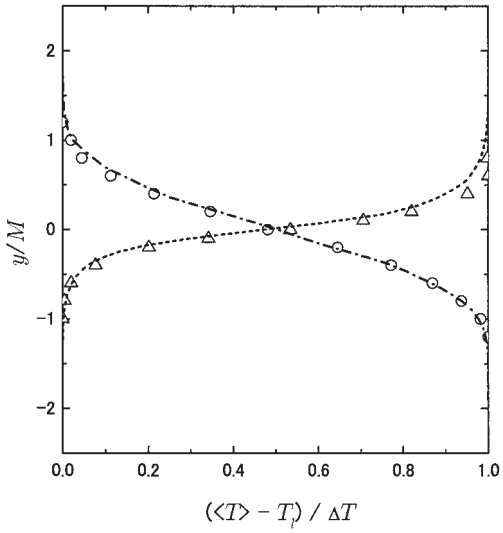

Figure 6. Vertical distributions of the mean temperature at $x/M = 20$ in the grid-generated turbulence.

Symbols denote the measurements and lines denote the LES predictions: △, - - -, in the unstably stratified case; ◇, – – –, in the stably stratified case.

the squared value of the cross-sectional mean velocity U_0^2. In the neutral case, the intensity decays following a power law with the exponent value of -1.58. The value compares well with values obtained in the previous grid-generated water flows.[14,16] The correlation coefficient between u and v, R_{uv} $[=\langle uv\rangle/(\sqrt{\langle u^2\rangle}\sqrt{\langle v^2\rangle})]$, was almost equal to zero in the whole region. The results show that ideal grid-generated turbulence is obtained in the neutrally stratified flow downstream of the turbulence-generating grid. Figure 5 also shows that the decay of the turbulence toward the downstream region is greater in the stably stratified case and smaller in the unstably stratified case. The LES predictions based on the two SGS stress models of Eqs. 6 and 7 are shown by two types of lines in the same figure together with the measurements. Hereafter we designate the two large-eddy simulations based on Eqs. 6 and 7 as LES(I) and LES(II), respectively. Although there is a little difference between the LES predictions and measurements in the upstream region of $x/M < 10$, they agree well in the downstream region. In the unstably and stably stratified cases, there is little difference between the two predictions by LES(I) and LES(II). This means that buoyancy does not directly affect the SGS flow field and we do not need to consider the buoyancy effect on the SGS Reynolds stress in the present flow. Therefore, the predictions only by LES(I) will be shown hereafter in this section.

Figure 6 shows the vertical distributions of the mean temperature at $x/M = 20$, normalized by the initial temperature difference. Typical unstable and stable thermal stratifications are formed and the LES predictions are in good agreement with the measurements. The Brunt–Väisälä frequency N is often used as an index to represent the stratification strength in isotropic turbulence. It is defined by $N = [(g/\rho_0)(\partial\langle\rho\rangle/\partial y)]^{1/2}$, where ρ_0 is the bulk-averaged density. The Brunt–Väisälä frequency estimated from Figure 6 corresponds to 1.40 rad/s in the stable case.

Figure 7 shows both the measurements and the LES predictions of the mixing layer width in the concentration field δ_c, defined by

$$\delta_c = |y_{c1} - y_{c2}|/0.8 \tag{20}$$

where $\langle C_A^*\rangle/C_{A0} = 0.9$ at y_{c1} and $\langle C_A^*\rangle/C_{A0} = 0.1$ at y_{c2}. It can be seen that the mixing region in the concentration field is

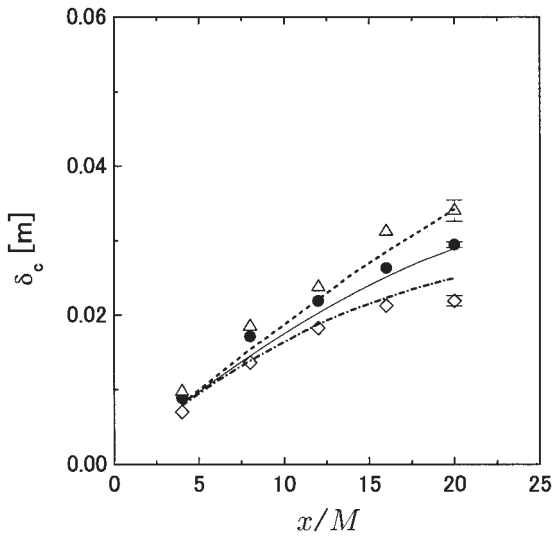

Figure 7. Streamwise distributions of the mixing layer width in the concentration field in the grid-generated turbulence.

Symbols denote the measurements and lines denote the LES predictions: ●, —, in the neutrally stratified case; △, - - -, in the unstably stratified case; ◇, – – –, in the stably stratified case. The error bars for the symbols indicate the standard deviations of the data at $x/M = 20$.

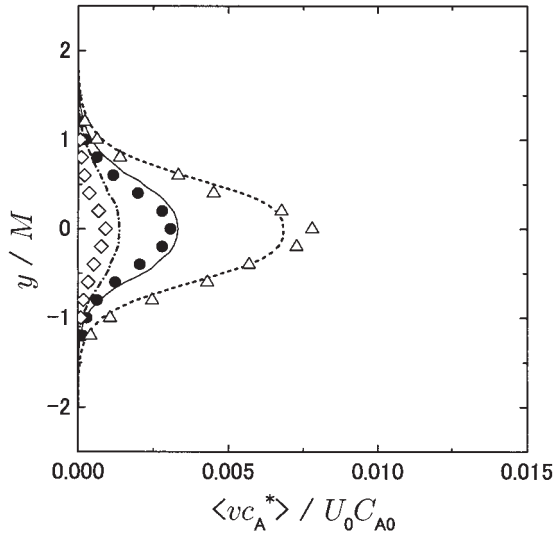

Figure 8. Vertical distributions of the vertical mass flux at $x/M = 20$ in the grid-generated turbulence.

Symbols and lines as in Figure 7.

vertically expanded by buoyancy in the unstably stratified case and reduced in the stably stratified case. This means that the turbulent mixing is promoted in the unstably stratified case and suppressed in the stably stratified case. Comparisons between LES predictions and measurements show that the LES can predict the mixing process with good accuracy even in stratified flows.

Figure 8 shows the vertical distributions of the vertical mass flux at $x/M = 20$, normalized by the product of the cross-sectional mean velocity and initial concentration of species A, U_0C_{A0}. It is obvious that the mass transfer is promoted in the unstably stratified case and suppressed in the stably stratified case. These buoyancy effects on the mass transfer cause the changes of the mixing layer width in the concentration field shown in Figure 7.

Figure 9 shows the vertical distributions of the mean concentration of chemical product at $x/M = 20$, normalized by the initial concentration of species A. The mean concentration of chemical product was calculated by

$$\langle C_P\rangle/C_{A0} = 2(\langle C_A^*\rangle - \langle C_A\rangle)/C_{A0} \tag{21}$$

The distribution of the chemical product is vertically enlarged in the unstably stratified case and reduced in the stably stratified case. This means that the chemical reaction is promoted in the unstably stratified case and suppressed in the stably stratified case. However, the maximum value of the mean concentration of chemical product is almost independent of the stratifications. The LES well predicts the profiles of the mean concentrations of chemical product in the stratified flows as well as in the neutrally stratified flow.

Mixing layer

Figures 10a and 10b show the visualized concentration fields obtained by the experiment and by the LES in the neutrally stratified mixing layer. The typical vortex pattern of shear turbulence can be clearly seen in both figures. This suggests that the present LES correctly reproduces the process of large-scale mixing.

Figure 11 shows the streamwise distributions of the mixing layer width in the velocity field δ_u, defined by

$$\delta_u = |y_{u1} - y_{u2}|/0.8 \tag{22}$$

where $(\langle U\rangle - U_l)/\Delta U = 0.9$ at y_{u1} and $(\langle U\rangle - U_l)/\Delta U = 0.1$ at y_{u2}. The mixing layer width in the neutral case grows linearly in the region of $x > 0.15$ m. The gradient $d\delta_u/dx$ is about 0.076, which is close to 0.073 derived from the equation proposed by Mehta and Westphal[6] by substituting the velocity ratio ($r = U_l/U_h$). This means that the typical mixing layer is formed in the neutral case. On the other hand, δ_u is smaller in the stably stratified case, whereas δ_u is larger in the unstably stratified case. Predictions by LES(I) and LES(II) are shown in the same figure together with the measurements. Both LES predictions are in good agreement with the measurements and the two LES predictions are almost the same. This means that we do not need to consider the buoyancy effect on the SGS Reynolds stress in either the mixing layer or the grid-generated turbulence. Therefore, only the predictions by LES(I) will be shown hereafter.

Figure 12 shows the vertical distributions of the mean temperature at $x = 0.40$ m, normalized by the initial temperature difference ΔT. Here y_t is the vertical position with the mean temperature equivalent to the cross-sectional mean temperature. In the measurements, the center of the mixing region deviates slightly from the center of the cross section because of the finite width of the test section. Therefore, it is necessary to introduce the y_t when we compare the measurements with the numerical predictions in the mixing layer. The value of y_t increases in the downstream direction. However, the value is very small and is 2 mm even at $x = 0.40$ m. The mean

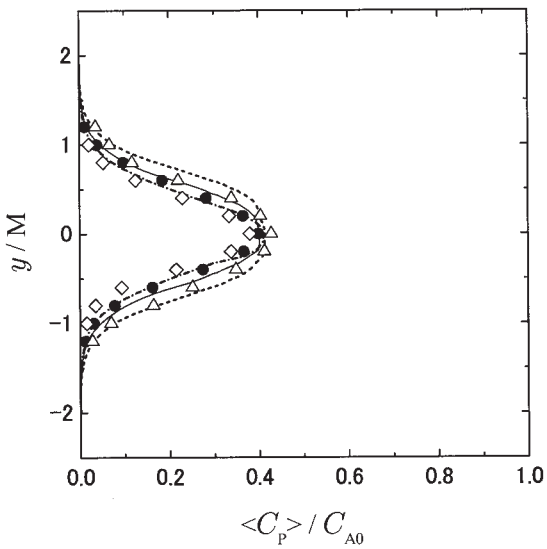

Figure 9. Vertical distributions of the mean concentration of chemical product at $x/M = 20$ in the grid-generated turbulence.

Symbols and lines as in Figure 7.

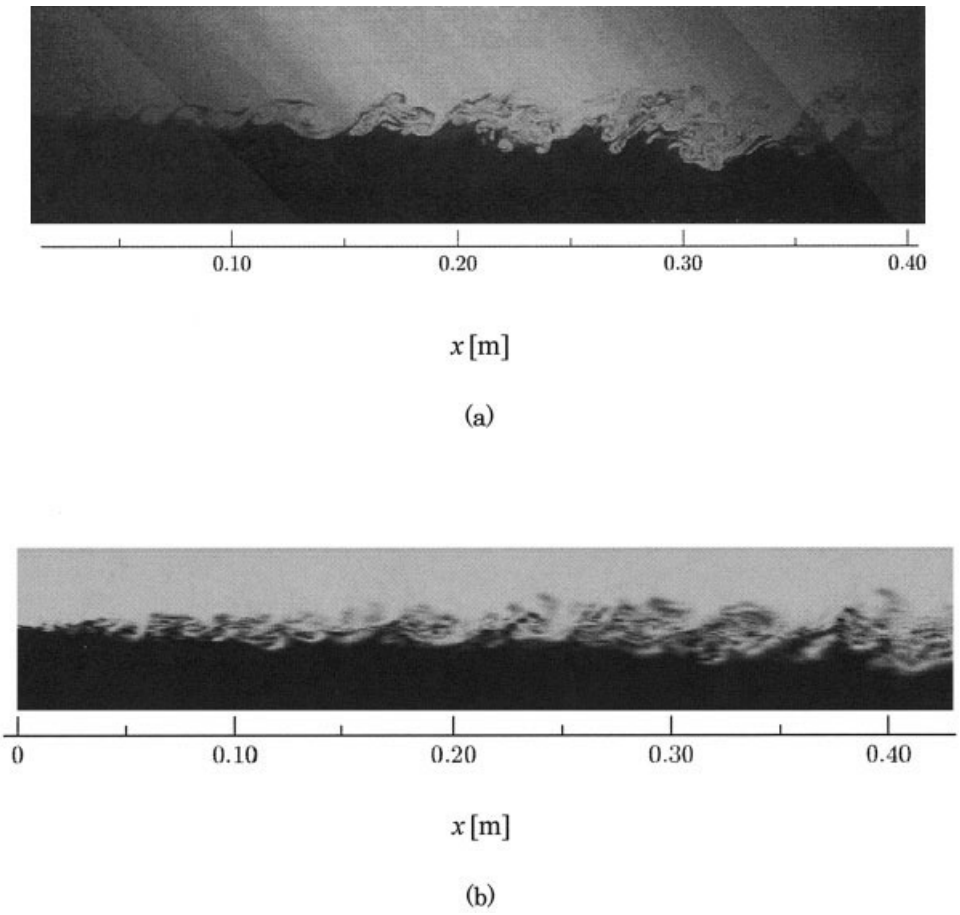

Figure 10. Instantaneous concentration field obtained (a) by the experiment with the LIF method and (b) by the LES, in the neutrally stratified mixing layer.

The upper stream is illuminated in both figures.

temperature profiles show that typical unstable and stable thermal stratifications are formed in both experiments and LES and that the present LES can well predict the mean temperature field as well as the mean velocity field.

Figure 13 shows the vertical distributions of the turbulence intensities of vertical velocity fluctuation at $x = 0.40$ m. Here the velocity fluctuations are normalized by the squared value of the initial velocity difference ΔU^2, and y_u is the vertical position where the mean velocity is equivalent to the cross-sectional mean velocity. It is found that the turbulence is promoted and suppressed in the unstably and stably stratified cases, respectively. The LES predictions are also in good agreement with the measurements. The agreements between the LES predictions and the measurements in Figures 11 and 13 prove that the present LES can accurately describe the thermal stratification effects on the velocity field.

A representative index of the strength of thermal stratification in the shear layer is given by the gradient Richardson number Ri_g, defined as

$$\mathrm{Ri}_g = -g\left(\frac{\partial \rho}{\partial y}\right) \Big/ \rho\left(\frac{\partial U}{\partial y}\right)^2 \tag{23}$$

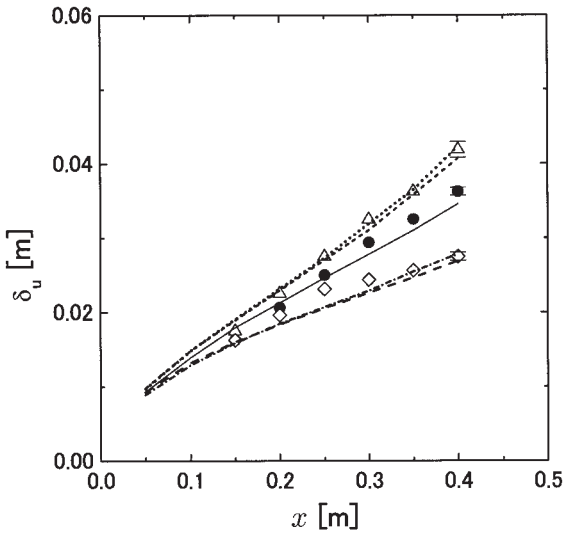

Figure 11. Streamwise distributions of the mixing layer width in the velocity field in the mixing layer.

Symbols and lines as in Figure 5. The error bars indicate the standard deviations of the data at $x = 0.40$ m.

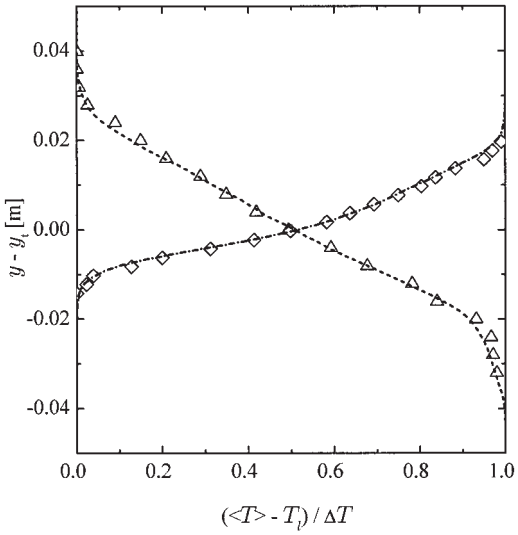

Figure 12. Vertical distributions of the mean temperature at $x = 0.40$ m in the mixing layer.

Symbols and lines as in Figure 6.

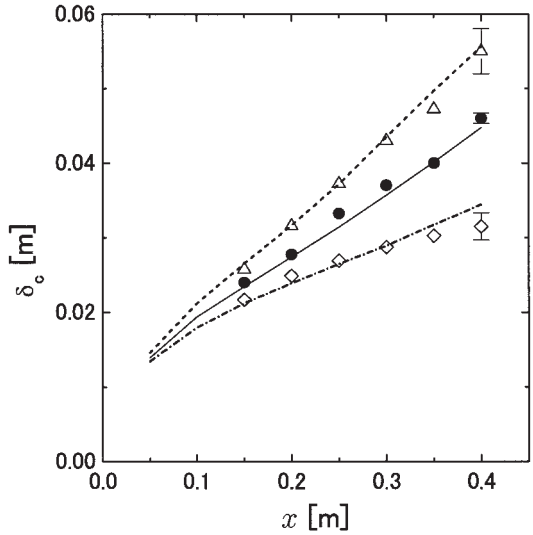

Figure 14. Streamwise distributions of the mixing layer width in the concentration field in the mixing layer.

Symbols and lines as in Figure 7. The error bars indicate the standard deviations of the data at $x = 0.40$ m.

where ρ is the density, g is gravity, U is the streamwise velocity, and y is the vertical distance. A suitable Richardson number for this experiment is

$$\mathrm{Ri}_g = -g\beta\Delta T\delta_u^2/\delta_t\Delta U^2 \tag{24}$$

where β is the thermal volumetric expansion coefficient and δ_t is the mixing layer width in the temperature field. The δ_t is defined as

$$\delta_t = |y_{t1} - y_{t2}|/0.8 \tag{25}$$

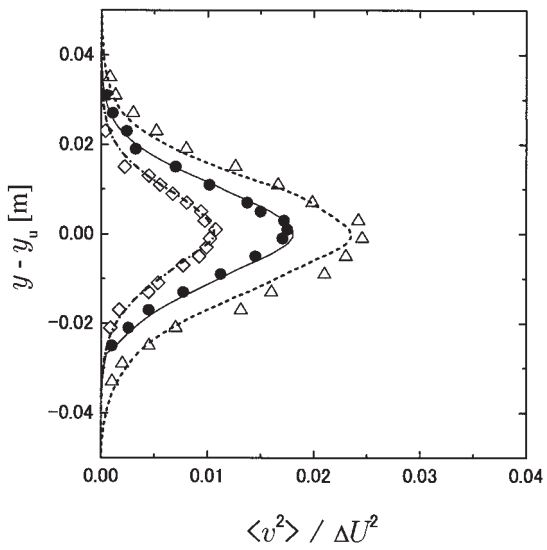

Figure 13. Vertical distributions of the turbulence intensity of vertical velocity fluctuation at $x = 0.40$ m in the mixing layer.

Symbols and lines as in Figure 7.

where $(\langle T\rangle - T_l)/\Delta T = 0.9$ at y_{t1} and $(\langle T\rangle - T_l)/\Delta T = 0.1$ at y_{t2}. The values of δ_u and δ_t at $x = 0.40$ m can be obtained from Figures 11 and 12, respectively. The value of Ri_g at $x = 0.40$ m estimated from the measurements is about -0.13 in the unstably stratified case and about 0.10 in the stably stratified case.

Figure 14 shows the streamwise distributions of the mixing layer width in the concentration field δ_c, defined by Eq. 20. The values of δ_c become larger in the unstably stratified case and smaller in the stably stratified case, which demonstrates the promotion and suppression of turbulent mixing by buoyancy. Comparisons between LES predictions and measurements show that the LES can predict the mixing process with good accuracy in the stratified cases as well as in the neutrally stratified case.

Figure 15 shows the vertical distributions of the vertical mass flux at $x = 0.40$ m, normalized by the product of the initial velocity difference and initial concentration of species A, ΔUC_{A0}. Here y_m is defined by the vertical position where the mean concentration of species A is equivalent to the cross-sectional mean concentration of species A. It can be seen that the mass transfer in the stratified cases is substantially changed by buoyancy. It should be noted that the vertical distributions of the mass flux are not symmetrical, although the vertical distributions of the velocity fluctuation shown in Figure 13 are symmetrical with respect to the axis of $y - y_u = 0$. This difference can be explained from the mean-squared value of the concentration fluctuation as shown in the next paragraph.

Figure 16a shows a visualized picture of turbulent mixing in the area of 0.10×0.10 m around $x = 0.40$ m in the neutrally stratified case. Here the upper stream with species B is illuminated and the black line in the photograph indicates the centerline of $y - y_m = 0$. Figure 16b shows the vertical distribution of the mean-squared value of the concentration fluctuation at $x = 0.40$ m in the neutrally stratified case, normalized by the squared value of the initial concentration of species A, C_{A0}^2.

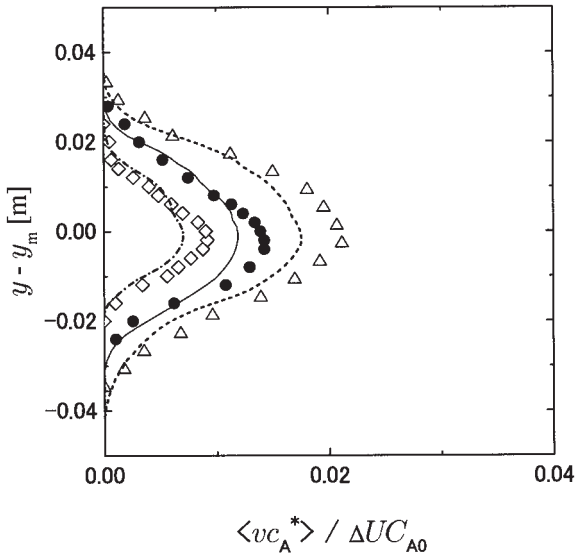

Figure 15. Vertical distributions of the vertical mass flux at $x = 0.40$ m in the mixing layer.

Symbols and lines as in Figure 7.

From this distribution, it is obvious that the intensity of the concentration fluctuation in the lower region is greater than that in the upper region. This can be explained from the photograph in Figure 16a, where a large concentration bulge is intruding into the lower region below the center line of $y - y_m = 0$. The larger concentration bulges promote the intensity of the concentration fluctuation and induce the asymmetry in the vertical mass flux as shown in Figure 16b.

In the LES, the mean-squared values of the concentration fluctuation $\langle c_A^{*2} \rangle$ was estimated by

$$\langle c_A^{*2} \rangle = \langle \overline{c_A^{*2}} \rangle + c_f \langle \widetilde{c_A^{*2}} \rangle \tag{26}$$

where $\langle \overline{c_A^{*2}} \rangle$ and $\langle \widetilde{c_A^{*2}} \rangle$ are the mean-squared values of normally filtered and test filtered concentration fluctuations, respectively, and c_f is the same coefficient of 5.0 as in Eq. 17. Michioka and Komori[4] warned that if we use the Cook–Riley[5] assumption of $c_f = 1.0$ appropriate for air turbulence, we underestimate the concentration fluctuation for liquid turbulence. On the other hand, the SGS fluctuations for the velocity fluctuation and mass flux could be neglected in Figures 13 and 15 because the large-scale eddies mainly play important roles in momentum and mass transfer, and therefore the contribution of SGS fluctuation to momentum and mass transfer is negligibly small. This is why the LES can accurately estimate the turbulence intensity and the mass flux from the GS values.

Figure 17 shows the vertical distributions of the mean concentration of chemical product P at $x = 0.40$ m, normalized by the initial concentration of species A, C_{A0}. The distribution of the chemical product is vertically enlarged in the unstably stratified case, that is, the chemical reaction is promoted by unstable stratification. In contrast, the chemical reaction is suppressed in the stably stratified case. However, the maximum values of the mean concentration of chemical product in all cases are almost the same. This trend is well predicted by the LES, although there is a slight difference between the LES predictions and measurements.

To explain the reason why the maximum value of $\langle C_P \rangle$ does not change, we calculated the power spectrum of the measured vertical velocity fluctuation E_W, defined by

$$\int_0^\infty E_{vv}(f)df = \langle v^2 \rangle \tag{27}$$

Figure 18 shows the power spectra of the vertical velocity fluctuation on the center line at $x = 0.40$ m. The high-frequency motion corresponds to the small-scale motion, and the low-frequency motion corresponds to the large-scale motion. The area bounded by the power spectrum multiplied by the frequency f

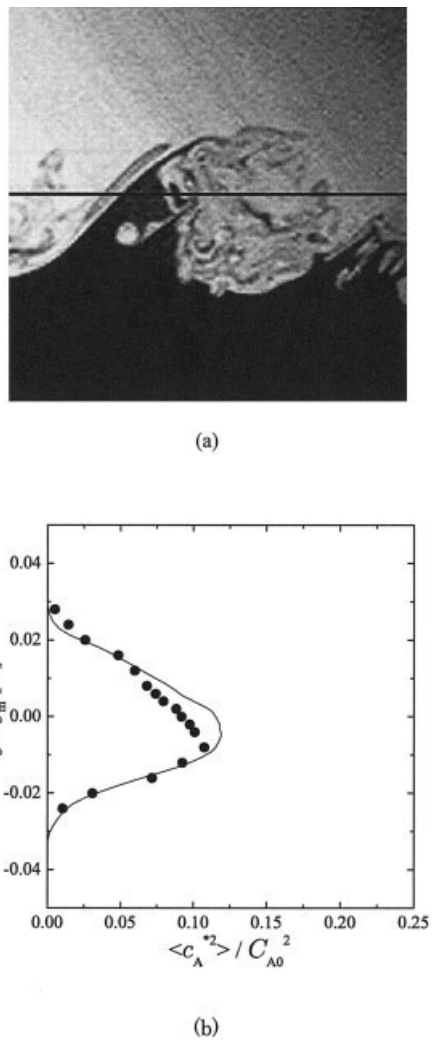

Figure 16. (a) A typical photograph of turbulent mixing in the area of 0.10 × 0.10 m² around $x = 0.40$ m and (b) vertical distributions of the mean-squared value of the concentration fluctuation at $x = 0.40$ m in the neutrally stratified mixing layer.

Symbol denotes the measurements and the line denotes the LES predictions.

corresponds to the intensity of the vertical velocity fluctuation. It should be noted that all the distributions reach their maximum values at about 2 Hz. The size of the eddy with 2 Hz is estimated to be about 3 cm with the Taylor's hypothesis. This eddy size is quite large compared to the Batchelor scale, which is approximately several tens of microns in liquid turbulence. Changes of the magnitude of power spectra arising from stratifications indicate that the low-frequency motions, that is, large-scale motions are sensitive to the buoyancy, whereas small-scale motions are insensitive. This fact coupled with the negligibly small buoyancy effects on the small-scale motion supports the assertion that large-scale flapping motions of the reacting interface are strongly affected by buoyancy, but the small-scale motions most responsible for the reaction in the interfacial area are not affected by buoyancy. This results in the maximum value of $\langle C_P \rangle$ in the central region independent of the thermal stratifications.

Conclusions

Laboratory experiments were carried out in two types of thermally stratified reacting liquid turbulence: grid-generated turbulence and a mixing layer. In addition, the LES with the SGS chemical reaction model developed by Michioka and Komori[4] was applied to the stratified reacting liquid flows, and the applicability of the LES was examined by comparisons with the measurements. The results from this study can be summarized as follows.

The turbulent mixing and chemical reaction are promoted by buoyancy in unstable stratification and suppressed in stable stratification. The maximum value of the mean concentration of chemical product in the central region is almost independent of the thermal stratifications. This is attributed to the fact that the buoyancy effects on the SGS flow field for the LES are negligibly small in liquid turbulent flows. The LES based on the SGS chemical reaction model of Michioka and Komori[4] is applicable to thermally stratified reacting liquid flows.

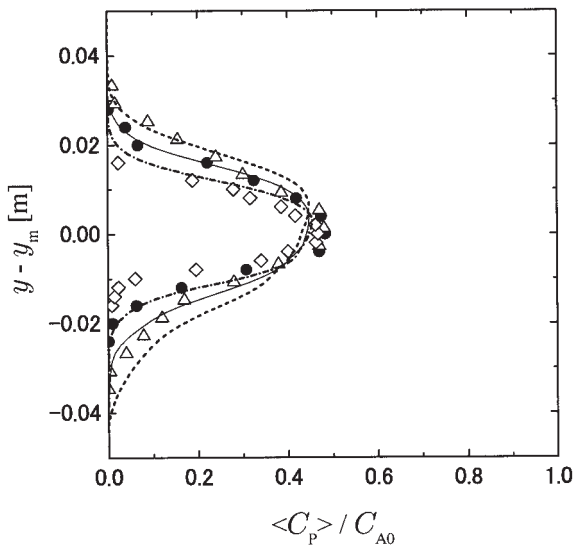

Figure 17. Vertical distributions of the mean concentration of the chemical product at x = 0.40 m in the mixing layer.

Symbols and lines as in Figure 7.

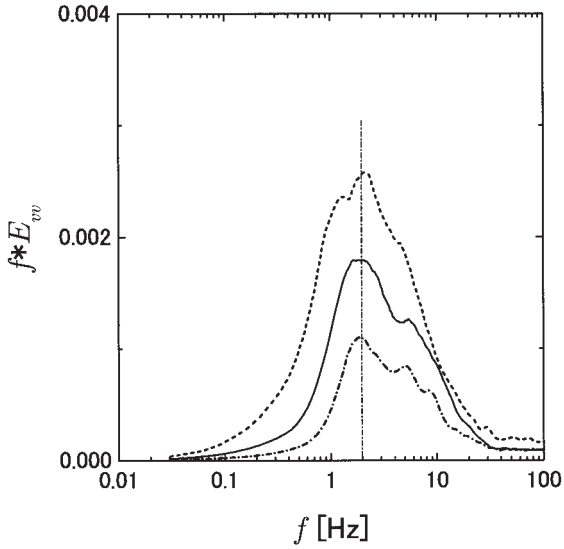

Figure 18. Measured power spectra of the vertical velocity fluctuation on the center line at x = 0.40 m in the mixing layer.

—, In the neutrally stratified case; - - -, in the unstably stratified case; – – –, in the stably stratified case.

These results are expected to be useful for designing chemical plants or reactors associated with liquid-phase reaction and heat transfer.

Acknowledgments

This research was supported by the Ministry of Education, Science, Sports and Culture, Grant-in-Aid (No.14102016) and the 21st Century Center of Excellence Program for Research and Education on Complex Functional Mechanical Systems. The numerical simulations were carried out by using a parallel supercomputer (NEC:SX-6) of the Center for Global Environment Research, National Institute for Environmental Studies, Environmental Ministry of Japan.

Notation

$B(a, b)$ = beta function
c_f = correlation coefficient in Eq. 17 (=5.0: constant)
C_i = concentration of chemical species i
d = thickness of a square rod
h_j = subgrid-scale heat flux
k_r = chemical reaction rate constant
L = representative length scale
M = mesh size of a turbulence-generating grid
N = Brunt–Väisälä frequency
P = pressure
$P(\zeta)$ = probability density function of ζ
Pr = Prandtl number
$\langle q^2 \rangle$ = turbulent kinetic energy
q_{ij} = subgrid-scale mass flux
R_{uv} = normalized Reynolds stress $[=\langle uv \rangle/(\sqrt{u^2}\sqrt{v^2})]$
Re = Reynolds number
Ri = Richardson number
Sc = Schmidt number
t = time
T_s = standard temperature
U_0 = cross-sectional mean velocity
U_i = velocity vector in the i-direction
Z = conserved scalar $(=C_A - C_B)$

Greek letters

ω = chemical reaction source term
τ_{ij} = subgrid-scale stress
$\tilde{\zeta}$ = normalized conserved scalar [$=(Z - Z_{B0})/(Z_{A0} - Z_{B0})$]
$\widetilde{\zeta''^2}$ = subgrid-scale variance of conserved scalar
$\widetilde{\gamma_i''^2}$ = subgrid-scale variance of chemical species i
$\tilde{\Delta}$ = computational grid width of the LES
Δt = time step

Subscripts

A = chemical species A
B = chemical species B
P = chemical production P
0 = initial value

Other symbols

$\langle \cdot \rangle$ = time-averaged value
$\bar{\ }$ = filtered value

Literature Cited

1. Nagata K, Komori S. The effects of unstable stratification and mean shear on the chemical reaction in grid turbulence. *J Fluid Mech.* 2000;408:39-52.
2. Koochesfahani MM, Dimotakis PE. Mixing and chemical reactions in a turbulent liquid mixing layer. *J Fluid Mech.* 1986;170:83-112.
3. Broadwell JE, Mungal MG. Large-scale structures and molecular mixing. *Phys Fluids A.* 1991;3:1193-1206.
4. Michioka T, Komori S. Large-eddy simulation of a turbulent reacting liquid flow. *AIChE J.* 2004;50:2705-2720.
5. Cook WA, Riley JJ. A subgrid model for equilibrium chemistry in turbulent flows. *Phys Fluids A.* 1994;6:2868-2870.
6. Mehta DR, Westphal VR. Near-field turbulence properties of single- and two-stream plane mixing layers. *Exp Fluids.* 1986;4:257-266.
7. Browand KF, Latigo OB. Growth of the two-dimensional mixing layer from a turbulent and nonturbulent boundary layer. *Phys Fluids A.* 1979;22:1011-1019.
8. Komori S, Kanzaki T, Murakami Y. Simultaneous measurements of instantaneous concentrations of two reacting species in a turbulent flow with a rapid reaction. *Phys Fluids A.* 1991;3:507-510.
9. Komori S, Nagata K, Kanzaki T, Murakami Y. Measurements of mass flux in a turbulent liquid flow with a chemical reaction. *AIChE J.* 1993;39:1611-1620.
10. Germano M, Piomelli U, Moin P, Cabot HW. A dynamic subgrid-scale eddy viscosity model. *Phys Fluids A.* 1991;3:1760-1765.
11. Wong CV, Lilly KD. A comparison of two dynamic subgrid closure methods for turbulent thermal convection. *Phys Fluids A.* 1994;6: 1016-1023.
12. Girimaji SS. Assumed β-pdf model for turbulent mixing. *Combust Sci Technol.* 1991;78:177-196.
13. Hirt CW, Cook JL. Calculating three-dimensional flows around structures and over rough terrain. *J Comp Phys.* 1972;10:324.
14. Nagata K, Komori S. The difference in turbulent diffusion between active and passive scalars in stable thermal stratification. *J Fluid Mech.* 2001;430:361-380.
15. Spalart RP. Direct simulation of a turbulent boundary layer up to $R_\theta = 1410$. *J Fluid Mech.* 1988;187:61-98.
16. Huq P, Britter RE. Mixing due to grid-generated turbulence of a two-layer scalar profile. *J Fluid Mech.* 1995;285:17-40.

Manuscript received July 16, 2004, and revision received July 22, 2005.